AGU PUBLICATIONS

Geophysical Research Letters

RESEARCH LETTER
10.1002/2016GL069430

Key Points:
- Thee-dimensional magnetic data sets from the autonomous underwater vehicle Sentry
- Subseafloor geometry of the ASHES vent field and its upflow zone
- Implications for the geophysical exploration of other vent sites

Correspondence to:
F. Caratori Tontini,
f.caratori.tontini@gns.cri.nz

Citation:
Caratori Tontini, F., T. J. Crone, C. E. J. de Ronde, D. J. Fornari, J. C. Kinsey, E. Mittelstaedt, and M. Tivey (2016), Crustal magnetization and the subseafloor structure of the ASHES vent field, Axial Seamount, Juan de Fuca Ridge: Implications for the investigation of hydrothermal sites, *Geophys. Res. Lett.*, *43*, 6205–6211, doi:10.1002/2016GL069430.

Received 2 MAY 2016
Accepted 3 JUN 2016
Accepted article online 7 JUN 2016
Published online 24 JUN 2016

Crustal magnetization and the subseafloor structure of the ASHES vent field, Axial Seamount, Juan de Fuca Ridge: Implications for the investigation of hydrothermal sites

Fabio Caratori Tontini[1], Timothy J. Crone[2], Cornel E. J. de Ronde[1], Daniel J. Fornari[3], James C. Kinsey[3], Eric Mittelstaedt[4], and Maurice Tivey[3]

[1]GNS Science, Lower Hutt, New Zealand, [2]Lamont-Doherty Earth Observatory, Columbia University, Palisades, New York, USA, [3]Woods Hole Oceanographic Institution, Woods Hole, Massachusetts, USA, [4]University of Idaho, Moscow, Idaho, USA

Abstract High-resolution geophysical data have been collected using the Autonomous Underwater Vehicle (AUV) *Sentry* over the ASHES (Axial Seamount Hydrothermal Emission Study) high-temperature (~348°C) vent field at Axial Seamount, on the Juan de Fuca Ridge. Multiple surveys were performed on a 3-D grid at different altitudes above the seafloor, providing an unprecedented view of magnetic data resolution as a function of altitude above the seafloor. Magnetic data derived near the seafloor show that the ASHES field is characterized by a zone of low magnetization, which can be explained by hydrothermal alteration of the host volcanic rocks. Surface manifestations of hydrothermal activity at the ASHES vent field are likely controlled by a combination of local faults and fractures and different lava morphologies near the seafloor. Three-dimensional inversion of the magnetic data provides evidence of a vertical, pipe-like upflow zone of the hydrothermal fluids with a vertical extent of ~100 m.

1. Introduction

Axial Seamount Hydrothermal Emission Study (ASHES) is an active hydrothermal vent field located near the southwestern caldera wall of Axial Seamount [e.g., *Hammond*, 1990; *Hammond and Delaney*, 1985; *Desonie and Duncan*, 1990; *Embley et al.*, 1990], ~300 km from the Oregon coast at the intersection of the Juan de Fuca Ridge and the Cobb-Eickelberg Seamount Chain [*Embley et al.*, 1990].

The elongated shape of Axial caldera (Figure 1) reflects the combined effect of a radial stress pattern (i.e., the Cobb-Eickelberg hot spot) with a linear stress field (i.e., the Juan de Fuca mid-ocean ridge) [e.g., *Delaney et al.*, 1981; *Crane et al.*, 1985; *Embley et al.*, 1990]. Axial Seamount has experienced several recent eruptions (i.e., 1998, 2011, and 2014), with the first real-time visual observations made in 1998 [e.g., *Baker et al.*, 1999; *Embley et al.*, 1999]. Subsequent to the 1998 eruption, Axial Seamount has been continuously monitored and has shown a pattern of inflation-deflation cycles which allowed *Chadwick et al.* [2006] and *Nooner and Chadwick* [2009] to predict an eruption event before 2014/2020; eruptions have since occurred in 2011 and again in 2014 [e.g., *Caress et al.*, 2012; *Chadwick et al.*, 2012; *Dziak et al.*, 2012].

The Axial Seamount lavas are mid-ocean ridge basalt showing some composition differences relative to other lavas along the rest of the Juan de Fuca Ridge [*Rhodes et al.*, 1990]. The complex volcanic history of this volcano is reflected in the intracaldera distribution of eruptive vents/fissures and variations in lava types (pillow, lobate, ropy, and jumbled sheet) [e.g., *Embley et al.*, 1990; *Hammond*, 1990; *Karsten and Delaney*, 1991; *Chadwick et al.*, 2005; *Clague et al.*, 2013].

Low-temperature hydrothermal venting at Axial Seamount was discovered in 1983 at the CASM (Canadian American Seamount Expedition) field [*Canadian American Seamount Expedition*, 1985; *Hammond*, 1990], and high-temperature venting was first observed in 1984 in the southwest part of the caldera inside the ASHES vent field [*Malahoff et al.*, 1984; *Baker et al.*, 1990; *Hammond*, 1990].

Axial Seamount has since then been mapped in detail, and hydrothermal vents and associated mineralization have been discovered in several places near the caldera [e.g., *Hannington and Scott*, 1988; *Massoth et al.*, 1989; *Hammond*, 1990; *Embley et al.*, 1990; *Feely et al.*, 1990; *Clague et al.*, 2013]. Very intense, short-term (<3 weeks) hydrothermal activity was also measured at the SONNE vent field simultaneously with the volcanic eruption of 1998 [*Baker et al.*, 1999].

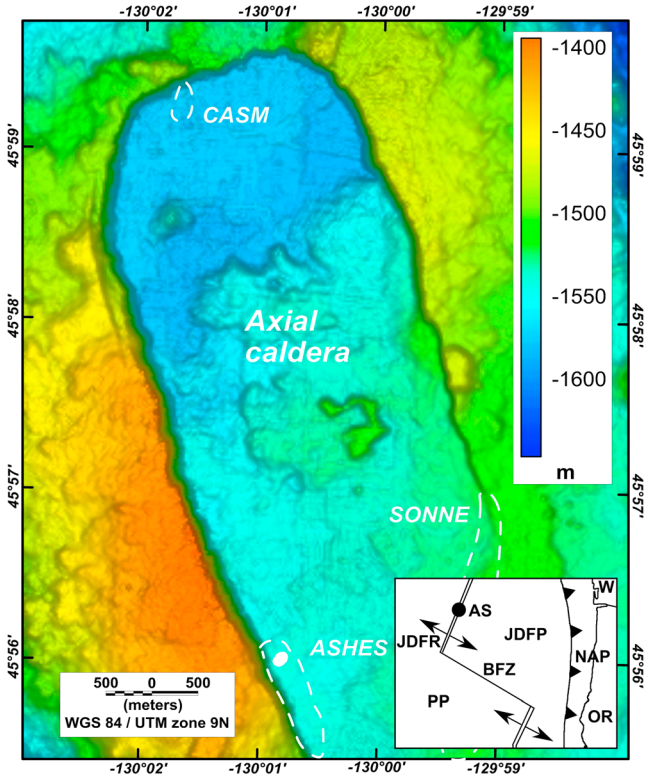

Figure 1. Map of Axial caldera and location of the ASHES, CASM, and SONNE vent fields (white dashed lines). The solid white circular area located inside the ASHES vent field indicates the area of high-temperature venting (Figure 2), over which magnetic survey was conducted. EM300 bathymetric data sets used in the Axial grid compilation are from the MBARI Cleft-Axial (1998) cruise and from the following NOAA VENTS cruises: TN149 (2002), TN160 (2003), TN173 (2004), TN199 (2006), and TN253 (2010). Inset shows the location of Axial Seamount (AS), Juan de Fuca Ridge (JDFR), Blanco Fracture Zone (BFZ), Cascadia subduction zone (line with triangles), the Oregon (OR) and Washington (W) States, and Pacific (PP), Juan de Fuca (JDFP), and North American (NAP) tectonic plates [*Bird*, 2003].

ASHES is characterized by a $1000 \times 200\ m^2$ area (Figure 1) of mostly low-temperature (<35°), diffuse venting [*Hammond*, 1990; *Embley et al.*, 1990; *Butterfield et al.*, 1990, 2004]. However, an almost circular area ~100 m diameter located at the northern end of the vent field (solid white circle in Figure 1) is characterized by high-temperature (up to 348°C), vigorous venting (Figure 2) together with extensive diffuse flow [*Butterfield et al.*, 1990; *Kelley et al.*, 2014; *Mittelstaedt et al.*, 2016].

Faulting along the caldera wall appears to provide the main structural control to the ASHES vent field [*Embley et al.*, 1990]. While low-temperature venting has been found on the caldera wall, adjacent to the high-temperature area shown in Figure 2 and in some places at the intersection between the caldera wall and caldera floor [*Embley et al.*, 1990], most venting occurs relatively far from the caldera walls, implying that other subsurface and local permeability controls shape the hydrothermal system at ASHES. For example, intense, focused venting correlates with a spatial distribution of lava types (i.e., sheet flows and pillow flows) that have inherently different permeabilities [*Hammond*, 1990].

Previous geophysical investigations at Axial Seamount consisted of shipborne magnetic surveying [*Tivey and Johnson*, 1990] and similarly, surveying gravity from sea level and on the seafloor [*Hildebrand et al.*, 1990]. These studies showed the existence of large areas of both low magnetization and low density, which are consistent with the presence of an active magma chamber and zones of highly porous, hydrothermally altered crust. More recently, near-seafloor gravity data were collected at the ASHES vent field by *Gilbert et al.* [2007] that show a correlation between low-density anomalies and the presence of hydrothermal alteration.

1.1. Seafloor Magnetic Surveys: Acquisition and Processing

Magnetic data were collected by *Sentry* [*Kinsey et al.*, 2011] using a detailed, 3-D grid over the high-temperature venting area at ASHES (Figure 2; *Sentry* dives #271–275), during a joint Deep Submergence Vehicle *Alvin*/AUV *Sentry* cruise on board the R/V *Atlantis* in July 2014.

Four grids with the same lateral extent were collected at different altitudes (10, 20, 40, and 60 m) above the seafloor (Figure 3a), because one of the main objectives of the *Sentry* mission was to perform accurate measurement of the overall hydrothermal heat and volume flux from the ASHES vent field by measuring temperature anomalies at different elevations.

It is interesting to note that potential field theory predicts that complete knowledge of magnetic field on an infinite horizontal surface is sufficient information to calculate the magnetic field at higher elevation by a process known as upward continuation [e.g., *Blakely*, 1995, and references therein]. At ASHES, however, we compared upward continued anomalies at 20–40 and 60 m with the observations and they are not identical. The theory

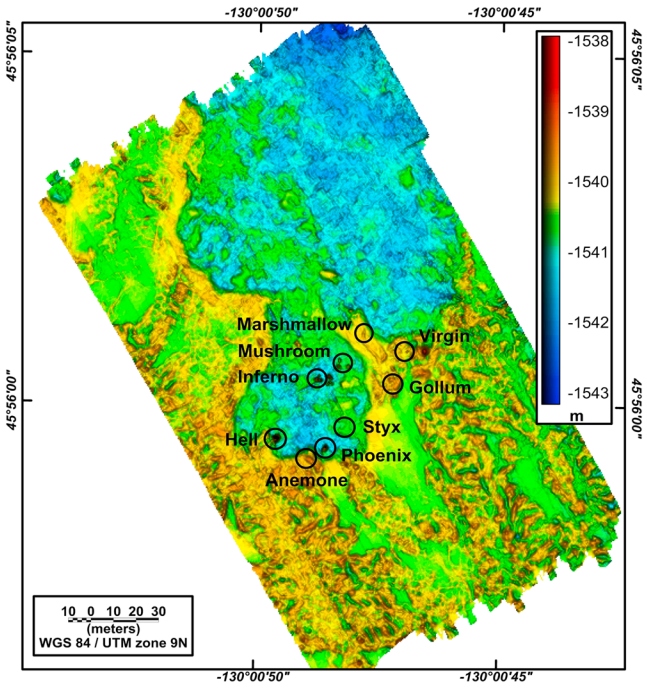

Figure 2. Map of the high-resolution (0.25 m) bathymetry of the survey area, with high-temperature vents (black circles). The solid white circular area located inside the ASHES vent field in Figure 1 encompasses the high-temperature vents. The bathymetry was collected at an altitude of 10 m above the seafloor using a RESON 7125 Seabat Sonar.

fails to accurately predict the observations because the effect of the regional magnetic field is not properly described in the small survey area which is far from being an infinite horizontal surface.

The data were corrected for the magnetic effect produced by the vehicle by measuring the magnetic field of the vehicle during the ascent/descent to and from the seafloor [e.g., *Tivey and Johnson*, 2002; *Caratori Tontini et al*., 2012a]. The magnetic data were not corrected for the diurnal correction because no base station data were available in proximity of the survey area [e.g., *Faggioni and Caratori Tontini*, 2002]. However, the Victoria Intermagnet Observatory shows that the survey was conducted during magnetically quiet days, with diurnal variation in the range ±50 nT, which is less than 2% of the amplitude of the magnetic anomalies measured over the ASHES vent field (Figure 3). Total intensity magnetic anomalies were obtained by subtracting a local polynomial reference field from the International Geomagnetic Reference Field [*Finlay et al*., 2010] and finally reduced to the magnetic pole.

The 10 m elevation magnetic anomaly grid (Figures 3b and 3c) was inverted to derive the distribution of subseafloor magnetization using the 3-D algorithm described in *Caratori Tontini et al*. [2012b]. This method is based on a discretization of the subseafloor into a 3-D grid of small prismatic cells so that a complex distribution of magnetization fitting the magnetic observations can be obtained.

This process is characterized by nonuniqueness and ambiguities which can be reduced by introducing external constraints in the inversion process, with a summary of the main constraints as follows:

1. The magnetization direction is assumed to be in the direction of the ambient geomagnetic field, i.e., inclination 66° and declination 16°.
2. Lower and upper bounds are imposed on the magnetization values in the range (0–10) A/m, which is a reasonable assumption for volcanic rocks younger than the last geomagnetic polarity reversal of ~0.7 Ma [*Johnson and Atwater*, 1977].
3. A sharp, focused solution is obtained by minimizing the misfit between observed and calculated anomalies and by minimizing the volume of the regions where the gradient of the magnetization distribution significantly differs from zero.

These constraints are particularly effective when mapping zones of hydrothermal alteration where we expect a sharp contact between hydrothermally altered zones and fresh volcanic rocks [*Caratori Tontini et al*., 2012b, 2013]. A 3-D magnetic model can be obtained from the inversion of the magnetic data in Figure 3 by using the 5 A/m magnetic isosurface (i.e., half of the magnetization range of 10 A/m) to delimit the upflow zone at the ASHES vent field (Figure 4).

2. Discussion

Near-seafloor magnetic surveys provide a unique method for mapping hydrothermal alteration in the submarine environment [e.g., *Tivey and Johnson*, 2002; *Tivey and Dyment*, 2010; *Tivey et al*., 2014; *Honsho et al*., 2013;

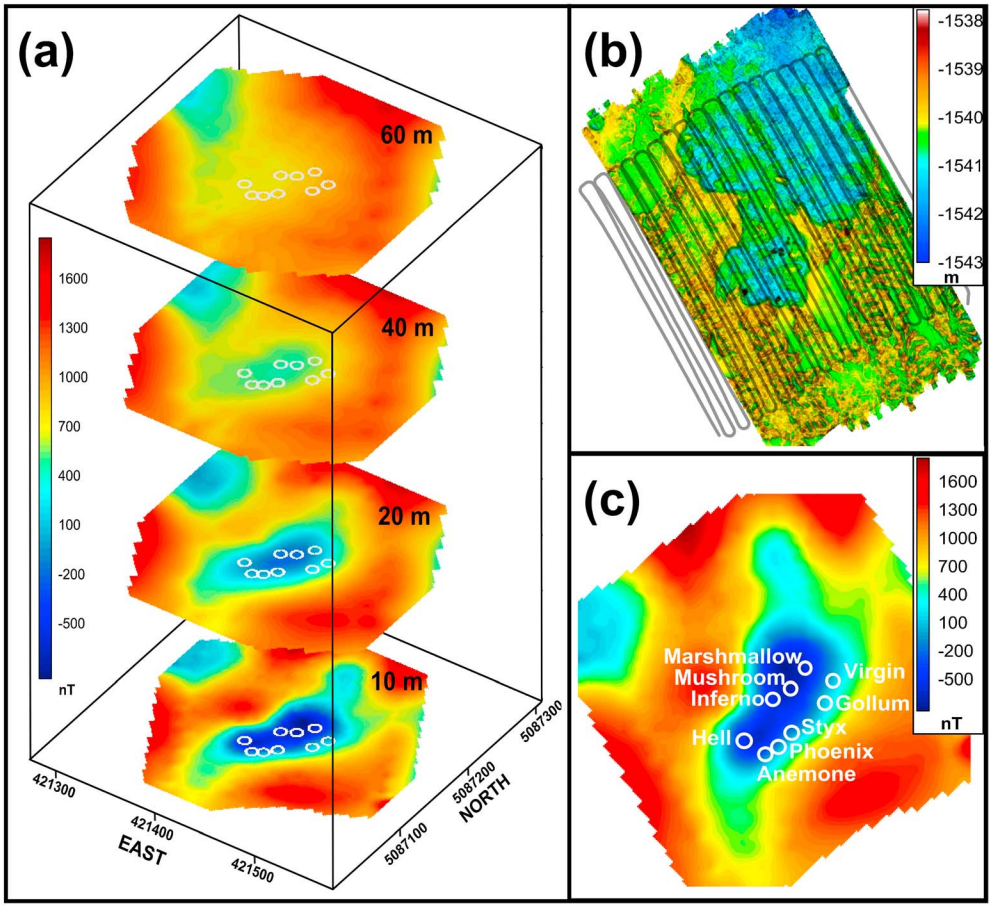

Figure 3. Three-dimensional magnetic anomaly with varying altitude above the seafloor and survey geometry (UTM zone 9 N projection, coordinate units are m). (a) Magnetic grids at 10, 20, 40, and 60 m above the seafloor, respectively. The white circles are the hydrothermal vents shown in Figure 2. (b) *Sentry* survey lines at 10 m above the seafloor. (c) Detail of the inverted magnetic grid at 10 m above the seafloor and high-temperature vents.

Fujii et al., 2015; *Szitkar et al.*, 2015a, 2015b]. Young oceanic crust is characterized by strong magnetization caused by magnetite and titanomagnetite minerals within the lavas. Water/rock interaction between hydrothermal fluids and the volcanic host rocks during fluid circulation can drastically reduce the magnetization of the host volcanic rocks as the magnetite is replaced by less magnetic minerals such as pyrite [e.g., *Ade-Hall et al.*, 1971; *Johnson and Atwater*, 1977; *Rona*, 1978]. Seafloor hydrothermal systems hosted in basaltic rock are, therefore, expected to be characterized by significant negative magnetic anomalies relative to the background [e.g., *Tivey et al.*, 2014; *Szitkar et al.*, 2015a].

This pattern is clearly visible in the 10 m altitude grid shown in Figure 3c, where a distinct negative magnetic anomaly of ~2000 nT amplitude is centered over the high-temperature vent sites of Figure 2. However, this negative anomaly becomes progressively less pronounced at higher altitudes above the seafloor; it is barely recognizable in the top grid at 60 m above the seafloor (Figure 3a). This effect is caused by the natural attenuation of the magnetic field with distance from the source. In the case of the ASHES vent field, an increase in the altitude of the vehicle from 10 m to 60 m above the seafloor prevents clear detection of the corresponding magnetic anomaly attributable to hydrothermal processes.

This strong decay of the amplitude of the magnetic field with increasing elevation also suggests that the demagnetized region caused by hydrothermal alteration is relatively shallow and thin. The distance at which the magnetic field decays is roughly of the same order as the depth interval in which the magnetic source is confined [*Pedersen*, 1991; *Tivey*, 1994; *Gee et al.*, 2001]. This can be seen in the 3-D magnetization model shown in Figure 4, where the depth range of the demagnetized body is ~100 m.

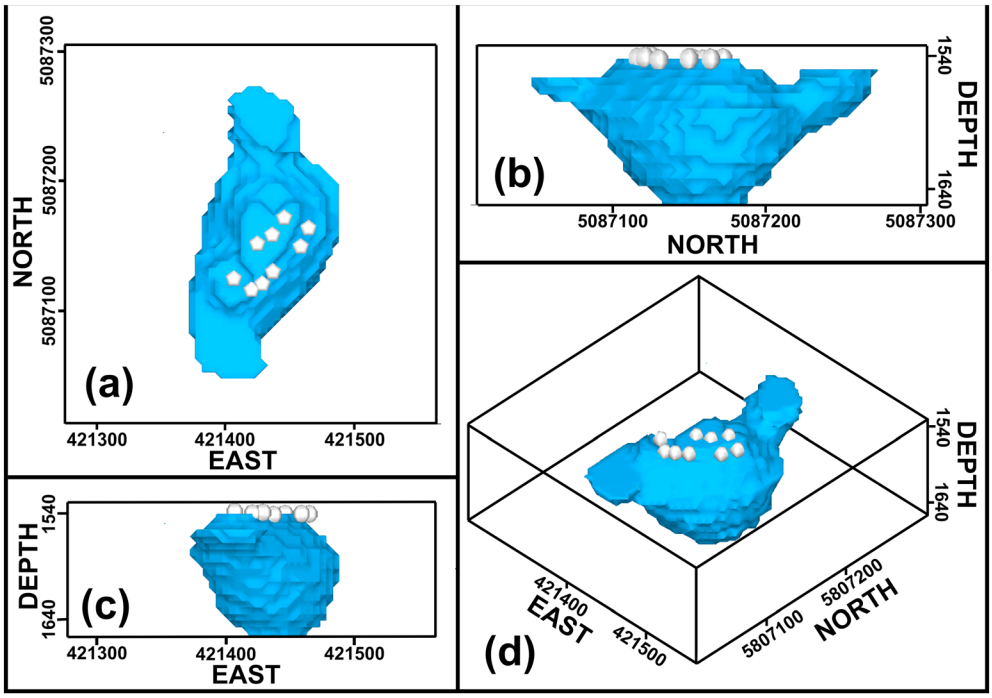

Figure 4. Three-dimensional model of the ASHES vent field (UTM zone 9 N projection, coordinates and depth units are m). A demagnetized zone is enclosed by the blue isosurface (5 A/m magnetization), while the white dots represent the high-temperature vents described in Figure 2. (a) Plan view, (b) view from the west, (c) view from the south, and (d) view from southeast.

The shape of the demagnetized body underlying the ASHES vent field is roughly elongated along a 15° azimuth relative to a N-S direction (Figure 4a), similar to the orientation of the observed magnetic anomaly in Figure 3c. This orientation is the same as the structural lineations marking segmented faulting that has been observed elsewhere in the caldera wall and floor and is parallel to the spreading axis of the Juan de Fuca Ridge [*Embley et al*., 1990; *Hammond*, 1990]. This seems to indicate linear stresses with a "rifting" component. The location of the vent site close to the caldera wall suggests, however, that high-permeability zones associated with caldera faults are also primary conduits for the vent fluids, together with other large-scale permeability structures (e.g., fissures and buried fissures).

A smaller and shallower inclined demagnetized upflow zone is located 50 m north of the main hydrothermally altered body situated under the high-temperature vents. This might be the magnetic expression of the lateral migration of hydrothermal fluids with significant mixing with cold seawater, supporting an area of widespread diffuse venting characterized by cracks and the accumulation of iron-rich silicate deposits [*Embley et al*., 1990; *Hammond*, 1990]. The shape of this lateral upflow zone is similar to the Brothers Volcano hydrothermal system in the Kermadec arc [e.g., *de Ronde et al*., 2005; *Embley et al*., 2012], where diffuse vent sites are defined by subseafloor demagnetized regions which are shallow, inclined conduits that merge with vertical, pipe-like demagnetized conduits underlying the focused, high-temperature vent sites [*Caratori Tontini et al*., 2012b].

The natural decay of the magnetic anomalies amplitude with increasing altitude above the seafloor in Figure 3 is accompanied by a northwest oriented migration and mixing with a lateral negative anomaly, which is only partly visible on the grids. The persistence of this anomaly at higher altitudes implies that it is generated by a deeper source. Additional data collected on a larger area are required to properly define and interpret this anomaly. One possible explanation is that it may represent a deeper connection with the caldera wall faults located west of the ASHES vent site, which provides a deep pathway for the upflow of hydrothermal fluids from the magma chamber and water/rock reaction zone under Axial Seamount.

3. Conclusion

The analysis of seafloor magnetic anomalies provides an effective tool to determine the geometry of upflow zones underlying hydrothermal vents. However, the depth resolution is limited by the natural decay of the magnetic field with increasing distance from the source. This effect can be clearly seen at the ASHES vent field, where magnetic data collected by an AUV utilizing excellent navigational control, using different grids at different altitudes above the seafloor, show a dramatic reduction of information once altitudes of 40–60 m above the seafloor are reached.

At ASHES it was possible to map the hydrothermal vent site with the necessary resolution because of the relatively flat bathymetry in the survey area. In other places, such as submarine volcanoes in subduction-related volcanic arcs, this is complicated by the rough terrain. Our results show that in order to detect and map in detail a hydrothermal site of similar size to ASHES, an altitude of 10–20 m above the seafloor is required for the best precision and accuracy of the magnetic anomaly which then means that a much smaller area will be convered during each AUV dive.

The ASHES 3-D magnetization model obtained from inversion of the magnetic data clearly shows the presence of a demagnetized region underlying the high-temperature vent sites. The shape of the demagnetized body suggests that a structural component parallel to rifting is driving the development of the high-temperature venting site. The depth resolution of the magnetic anomalies and the location close to the caldera faults suggests that the ASHES vent field is also structurally controlled by faulting along the caldera walls which provide deep pathways for the upflow of hydrothermal fluids from the reaction zone.

Acknowledgments

The paper has greatly benefited from the review by Rick Blakely and Luca Cocchi. We thank the Captain and crew of the R/V *Atlantis* for the safe deployment and recovery of the AUV *Sentry*. We also thank Alan Duester, Justin Fujii, Johanna Hansen, and Zac Berkowitz for the successful operation of *Sentry* during this cruise. The magnetic data and grids shown in this paper are archived at the Marine Geoscience Data System (MGDS, www.marine-geo.org), which is part of the Integrated Earth Data Alliance (IEDA) online database. This work was supported by the Royal Society of New Zealand (Marsden grant GNS1003) and the New Zealand Ministry of Business, Innovation and Employment (MBIE) core funding to GNS Science and NSF grants OCE-1131455 to T.C., OCE-1337473 to J.K., and OCE-1131772 to E.M. and D.F.

References

Ade-Hall, J. M., H. C. Palmer, and T. P. Hubbard (1971), The magnetic and opaque petrological response of basalt to regional hydrothermal alteration, *Geophys. J. R. Astron. Soc.*, *24*, 137–174.

Baker, E. T., R. E. McDuff, and G. J. Massoth (1990), Hydrothermal venting from the summit of a ridge-axis seamount: Axial volcano, Juan de Fuca Ridge, *J. Geophys. Res.*, *95*, 12,843–12,854, doi:10.1029/JB095iB08p12843.

Baker, E. T., C. G. Fox, and J. P. Cowen (1999), In situ observations of the onset of hydrothermal discharge during the 1998 submarine eruption of Axial Volcano, Juan de Fuca Ridge, *Geophys. Res. Lett.*, *26*, 3445–3448, doi:10.1029/1999GL002331.

Bird, P. (2003), An updated digital model of plate boundaries, *Geochem. Geophys. Geosyst.*, *4*(3), 1027, doi:10.1029/2001GC000252.

Blakely, R. J. (1995), *Potential Theory in Gravity and Magnetic Applications*, Cambridge Univ. Press, Cambridge, U. K.

Butterfield, D. A., G. J. Massoth, R. E. McDuff, J. E. Lupton, and M. D. Lilley (1990), Geochemistry of hydrothermal fluids from Axial Seamount hydrothermal emissions study vent field, Juan de Fuca Ridge: Subseafloor boiling and subsequent fluid-rock interaction, *J. Geophys. Res.*, *95*, 12,895–12,921, doi:10.1029/JB095iB08p12895.

Butterfield, D. A., K. K. Roe, M. D. Lilley, J. A. Huber, J. A. Baross, R. W. Embley, and G. J. Massoth (2004), Mixing, reaction, and microbial activity in the subseafloor revealed by temporal and spatial variation in diffuse flow vents at Axial Volcano, in *The Subseafloor Biosphere at Mid-Ocean Ridges*, *Geophys. Monogr. Ser.*, vol. 144, edited by W. S. D. Wilcock et al., pp. 269–289, AGU, Washington, D. C.

Canadian American Seamount Expedition (1985), Hydrothermal vents on the Axial Seamount on the Juan de Fuca Ridge, *Nature*, *313*, 212–214.

Caratori Tontini, F., B. Davy, C. E. J. de Ronde, R. W. Embley, M. Leybourne, and M. A. Tivey (2012a), Crustal magnetization of Brothers Volcano, New Zealand, measured by autonomous underwater vehicles: Geophysical expression of a submarine hydrothermal system, *Econ. Geol.*, *107*, 1571–1581.

Caratori Tontini, F., C. E. J. de Ronde, D. Yoerger, J. C. Kinsey, and M. A. Tivey (2012b), 3-D focused inversion of near-seafloor magnetic data with application to the Brothers Volcano hydrothermal system, Southern Pacific Ocean, New Zealand, *J. Geophys. Res.*, *117*, B10102, doi:10.1029/2012JB009349.

Caratori Tontini, F., C. E. J. de Ronde, J. C. Kinsey, A. Soule, D. Yoerger, and L. Cocchi (2013), Geophysical modeling of collapse-prone zones at Rumble III seamount, southern Pacific Ocean, New Zealand, *Geochem. Geophys. Geosyst.*, *14*, 4667–4680, doi:10.1002/ggge.20278.

Caress, D. W., D. A. Clague, J. B. Paduan, J. F. Martin, B. M. Dreyer, W. W. Chadwick Jr., A. Denny, and D. S. Kelley (2012), Repeat bathymetric surveys at 1-metre resolution of lava flows erupted at Axial Seamount in April 2011, *Nat. Geosci.*, *5*, 483–488.

Chadwick, J., M. Perfit, I. Ridley, I. Jonasson, G. Kanenov, W. Chadwick, R. Embley, P. le Roux, and M. Smith (2005), Magmatic effects of the Cobb hot spot on the Juan de Fuca Ridge, *J. Geophys. Res.*, *110*, B03101, doi:10.1029/2003JB002767.

Chadwick, W. W., Jr., S. Nooner, M. Zumberge, R. W. Embley, and C. G. Fox (2006), Vertical deformation monitoring at Axial Seamount since its 1998 eruption using deep-sea pressure sensors, *J. Volcanol. Geotherm. Res.*, *150*, 313–327.

Chadwick, W. W., Jr., S. L. Nooner, D. A. Butterfield, and M. D. Lilley (2012), Seafloor deformation and forecasts of the April 2011 eruption at Axial Seamount, *Nat. Geosci.*, *5*, 474–477.

Clague, D. D., et al. (2013), Geologic history of the summit of Axial Seamount, Juan de Fuca Ridge, *Geochem. Geophys. Geosyst.*, *14*, 4403–4443, doi:10.1002/ggge.20240.

Crane, K. F., F. Aikman, R. W. Embley, S. R. Hammond, A. Malahoff, and J. Lupton (1985), The distribution of geothermal fields on the Juan de Fuca Ridge, *J. Geophys. Res.*, *90*, 727–744, doi:10.1029/JB090iB01p00727.

Delaney, J. R., H. P. Johnson, and J. L. Karsten (1981), The Juan de Fuca Ridge-hot spot-propagating rift system: New tectonic, geochemical, and magnetic data, *J. Geophys. Res.*, *95*, 11,747–11,750, doi:10.1029/JB086iB12p11747.

de Ronde, C. E. J., et al. (2005), Evolution of a submarine magmatic-hydrothermal system: Brothers Volcano, Southern Kermadec Arc, New Zealand, *Econ. Geol.*, *100*(6), 1097–1133.

Desonie, D. L., and R. A. Duncan (1990), The Cobb-Eickelberg Seamount Chain: Hotspot volcanism with mid-ocean ridge basalt affinity, *J. Geophys. Res.*, *95*, 12,697–12,711, doi:10.1029/JB095iB08p12697.

Dziak, R. P., J. H. Haxel, D. R. Bohnenstiehl, W. W. Chadwick Jr., S. L. Nooner, M. J. Fowler, H. Matsumoto, and D. A. Butterfield (2012), Seismic precursors and magma ascent before the April 2011 eruption at Axial Seamount, *Nat. Geosci.*, *5*, 478–482.

Embley, R. W., K. M. Murphy, and C. G. Fox (1990), High-resolution studies of the summit of Axial Volcano, *J. Geophys. Res.*, *95*, 12,785–12,812, doi:10.1029/JB095iB08p12785.

Embley, R. W., W. W. Chadwick Jr., D. Clague, and D. Stakes (1999), 1998 eruption of Axial Volcano: Multibeam anomalies and seafloor observations, *Geophys. Res. Lett.*, *26*, 3425–3428, doi:10.1029/1999GL002328.

Embley, R. W., C. E. J. de Ronde, S. G. Merle, B. Davy, and F. Caratori Tontini (2012), Detailed morphology and structure of an active submarine arc caldera: Brothers Volcano, Kermadec Arc, *Econ. Geol.*, *107*(8), 1557–1570.

Faggioni, O., and F. Caratori Tontini (2002), Quantitative evaluation of the time-line reduction performance in high definition marine magnetic surveys, *Mar. Geophys. Res.*, *23*, 353–365.

Feely, R. A., T. L. Geiselman, E. T. Baker, and G. J. Massoth (1990), Distribution and composition of hydrothermal plume particles from the ASHES vent field at Axial volcano, Juan de Fuca Ridge, *J. Geophys. Res.*, *95*, 12,855–12,873, doi:10.1029/JB095iB08p12855.

Finlay, C. C., et al. (2010), International geomagnetic reference field: The eleventh generation, *Geophys. J. Int.*, *183*, 1216–1230.

Fujii, M., K. Okino, C. Honsho, J. Dyment, F. Szitkar, and M. Asada (2015), High-resolution magnetic signature of active hydrothermal systems in the back-arc spreading region of the Southern Mariana Trough, *J. Geophys. Res. Solid Earth*, *120*, 2821–2837, doi:10.1002/2014JB011714.

Gee, J., S. Webb, J. Ridgway, H. Staudigel, and M. Zumberge (2001), A deep tow magnetic survey of Middle Valley, Juan de Fuca Ridge, *Geochem. Geophys. Geosyst.*, *2*(11), 1059, doi:10.1029/2001GC000170.

Gilbert, L. A., R. E. McDuff, and H. P. Johnson (2007), Porosity of the upper edifice of Axial Seamount, *Geology*, *35*, 49–52.

Hammond, S. R. (1990), Relationships between lava types, seafloor morphology, and the occurrence of hydrothermal venting in the ASHES Vent Field of Axial Volcano, *J. Geophys. Res.*, *95*, 12,875–12,893, doi:10.1029/JB095iB08p12875.

Hammond, S. R., and J. P. Delaney (1985), Evolution of Axial Volcano, Juan de Fuca Ridge, *Eos Trans. AGU*, *6*, 925.

Hannington, M. D., and S. D. Scott (1988), Mineralogy and geochemistry of a silica-sulfate deposit in the caldera of Axial Seamount, N.E. Pacific Ocean, *Can. Mineral.*, *26*, 603–626.

Hildebrand, J. A., J. M. Stevenson, P. T. C. Hammer, M. A. Zumberge, R. L. Parker, C. G. Fox, and P. J. Meis (1990), A seafloor and sea surface gravity survey of Axial Volcano, *J. Geophys. Res.*, *95*, 12,751–12,763, doi:10.1029/JB095iB08p12751.

Honsho, C., T. Ura, and K. Kim (2013), Deep-sea magnetic vector anomalies over the Hakurei hydrothermal field and the Bayonnaise knoll caldera, Izu-Ogasawara arc, Japan, *J. Geophys. Res. Solid Earth*, *118*, 5147–5164, doi:10.1002/jgrb.50382.

Johnson, H. P., and T. Atwater (1977), Magnetic study of basalts from the mid-Atlantic ridge, lat. 37°N, *Geol. Soc. Am. Bull.*, *88*, 637–647.

Karsten, J. L., and J. P. Delaney (1991), Hot spot-ridge crest convergence in the northeast Pacific, *J. Geophys. Res.*, *96*, 4083–4105, doi:10.1029/90JB02364.

Kelley, D. S., J. R. Delaney, and S. K. Juniper (2014), Establishing a new era of submarine volcanic observatories: Cabling Axial Seamount and the Endeavour Segment of the Juan de Fuca Ridge, *Mar. Geol.*, doi:10.1016/j.margeo.2014.03.010.

Kinsey, J. C., D. R. Yoerger, M. V. Jakuba, R. Camilli, C. R. Fisher, and C. R. German (2011), Assessing the deepwater horizon oil spill with the Sentry autonomous underwater vehicle, in *Proceedings of the 2011 IEEE International Conference on Intelligent Robots and Systems, September 2011, San Francisco, CA*, pp. 261–267, IEEE, San Francisco, Calif., doi:10.1109/IROS.2011.6095008.

Malahoff, A., G. McMurtry, S. Hammond, and R. W. Embley (1984), High-temperature hydrothermal fields: Juan de Fuca Ridge—Axial Volcano, *Eos Trans. AGU*, *65*, 1112.

Massoth, G. J., D. A. Butterfield, J. E. Lupton, R. E. McDuff, M. D. Lilley, and I. R. Jonasson (1989), Submarine venting of phase-separated hydrothermal fluids at Axial Volcano, Juan de Fuca Ridge, *Nature*, *340*, 702–705.

Mittelstaedt, E., D. J. Fornari, T. J. Crone, J. Kinsey, D. Kelley, and M. Elend (2016), Diffuse venting at the ASHES hydrothermal field: Heat flux and tidally modulated flow variability derived from in situ time-series measurements, *Geochem. Geophys. Geosyst.*, *17*, 1435–1453, doi:10.1002/2015GC006144.

Nooner, S. L., and W. W. Chadwick Jr. (2009), Volcanic inflation measured in the caldera of Axial Seamount: Implications for magma supply and future eruptions, *Geochem. Geophys. Geosyst.*, *10*, Q02002, doi:10.1029/2008GC002315.

Pedersen, L. B. (1991), Relations between potential fields and some equivalent sources, *Geophysics*, *56*, 961–971.

Rhodes, J. M., C. Morgan, and R. A. Liias (1990), Geochemistry of Axial Seamount lavas: Magmatic relationship between the Cobb Hotspot and the Juan de Fuca Ridge, *J. Geophys. Res.*, *95*, 12,713–12,733, doi:10.1029/JB095iB08p12713.

Rona, P. A. (1978), Magnetic signatures of hydrothermal alteration and volcanogenic mineral deposits in oceanic crust, *J. Volcanol. Geotherm. Res.*, *3*, 219–225.

Szitkar, F., J. Dyment, Y. Fouquet, Y. Choi, and C. Honsho (2015a), Absolute magnetization of the seafloor at a basalt-hosted hydrothermal site: Insights from a deep-sea submersible survey, *Geophys. Res. Lett.*, *42*, 1046–1052, doi:10.1002/2014GL062791.

Szitkar, F., S. Petersen, F. Caratori Tontini, and L. Cocchi (2015b), High-resolution magnetics reveal the deep structure of a volcanic-arc-related basalt-hosted hydrothermal site (Palinuro, Tyrrhenian Sea), *Geochem. Geophys. Geosyst.*, *16*, 1950–1961, doi:10.1002/2015GC005769.

Tivey, M. A. (1994), High-resolution magnetic surveys over the Middle Valley mounds, Northern Juan de Fuca Ridge, *Proc. Ocean Drill. Program Sci. Results*, *139*, 29–35.

Tivey, M. A., and J. Dyment (2010), The magnetic signature of hydrothermal systems in slow spreading environments, in *Diversity of Hydrothermal Systems on Slow Spreading Ocean Ridges*, *Geophys. Monogr. Ser.*, vol. 188, edited by P. Rona, C. Devey, and B. Murton, pp. 43–65, AGU, Washington, D. C.

Tivey, M. A., and H. P. Johnson (1990), The magnetic structure of Axial Seamount, Juan de Fuca Ridge, *J. Geophys. Res.*, *95*, 12,735–12,750, doi:10.1029/JB095iB08p12735.

Tivey, M. A., and H. P. Johnson (2002), Crustal magnetization reveals subsurface structure of the Juan de Fuca Ridge hydrothermal vent fields, *Geology*, *30*, 979–982.

Tivey, M. A., H. P. Johnson, M. S. Salmi, and M. Hutnak (2014), High-resolution near-bottom vector magnetic anomalies over Raven Hydrothermal Field, Endeavour Segment, Juan de Fuca Ridge, *J. Geophys. Res. Solid Earth*, *119*, 7389–7403, doi:10.1002/2014JB011223.